Journal of Molecular Liquids 335 (2021) 116243

Contents lists available at ScienceDirect

Journal of Molecular Liquids

journal homepage: www.elsevier.com/locate/molliq

A molecular dynamics study of the effect of functional groups and side chain on adsorption of alcoholic surfactant and interfacial thermal transport

Yuting Guo [a,b,*], Donatas Surblys [b], Hiroki Matsubara [b], Taku Ohara [b]

[a] Department of Mechanical and Aerospace Engineering, Graduate School of Engineering, Tohoku University, Sendai 980-8579, Japan
[b] Institute of Fluid Science, Tohoku University, Sendai 980-8577, Japan

ARTICLE INFO

Article history:
Received 4 March 2021
Revised 13 April 2021
Accepted 18 April 2021
Available online 21 April 2021

Keywords:
Surfactant
Solid-liquid interface
Thermal boundary resistance
Adsorption structure

ABSTRACT

In the present study, we investigated the effect of the number and position of functional groups, and the length of the main chain and side chain in organic surfactant on adsorption behavior and interfacial heat transfer between silica surface and alkane solvent by non-equilibrium molecular dynamics simulation, where the surfactants were primary/secondary alcohol, monohydric/dihydric alcohol, and linear/branched alcohol. The results showed a similar adsorption behavior for all the surfactant types, where hydroxyl functional (—OH) groups adsorbed onto the silica surface and alkyl chain was in contact with the solvent, which produced a heat path from silica via surfactant to solvent. The number of adsorbed —OH groups did not directly translate to significantly decreased thermal boundary resistance due to the adsorption structure. Coulomb interaction enabled the closer distance between primary terminal —OH groups in surfactant and silica surface, which enhanced the solid-surfactant intermolecular heat transfer. However, Coulomb interaction contributed less to shorten the molecular distances between secondary —OH groups in surfactant and silica surface, which was connected to less efficient heat transfer from silica to surfactant and thereby did not enhance the interfacial heat transfer as much as surfactants with terminal —OH. The increase in terminal —OH groups in the surfactant molecules could not significantly reduce thermal boundary resistance, although the adsorption amount of —OH was distinctly greater than that of surfactants with single —OH. The side chain in surfactant enabled the efficient surfactant-solvent intermolecular heat transfer but related to the desorption of surfactant when decreasing the temperature. Thus branched-chain dihydric alcohol performed better than other surfactants on reducing thermal boundary resistance when the interfacial temperature was high enough to maintain the sufficient adsorption amount. We considered such reverse temperature-sensitive surfactant has a great potential application to fulfill multiple needs for heat dissipation of electronic devices, especially the high temperature operation. The new insights obtained in the present study were a step towards a molecular structure design of surfactant enhancing solid–liquid interfacial heat transfer.

1. Introduction

Large thermal resistance in power modules usually occurs at the joint interface due to the gap between individual electronic components. In order to reduce such thermal resistance, thermal interface materials (TIMs) with high thermal conductivity are used to fill the gaps between solid surfaces [1,2]. Due to miniaturization trends, many electronic components have reached nanoscale [3], and the bulk thermal resistance of ultra-thin TIMs applied between these electronic components has also become accordingly smaller. In such cases, the performance of TIMs becomes mostly dependent on the TIM-substrate thermal boundary resistance (R_b). Past works [4–7] showed that surface modification based on covalent bonds can be successfully applied to reduce R_b, while our previous studies [8–10] found that the surfactants based on physical adsorption can also reduce R_b in a simpler mechanism and is easier to apply. In one of these previous works, it was demonstrated that an increase in surfactant chain length could enhance the interfacial heat transfer when simple linear alcohols were used as a surfactant [10]. However, the influence of more complicated molecular configurations of polymer surfactant on interfacial thermal transfer remains

* Corresponding author.
E-mail addresses: guo@microheat.ifs.tohoku.ac.jp (Y. Guo), donatas@tohoku.ac.jp (D. Surblys), matsubara@microheat.ifs.tohoku.ac.jp (H. Matsubara), ohara@ifs.tohoku.ac.jp (T. Ohara).

https://doi.org/10.1016/j.molliq.2021.116243
0167-7322/

poorly understood. For surfactant molecules with different chain lengths and functional groups, a variety of adsorption structures can form on the solid surface [11–15], which might affect the interfacial heat transfer. The purpose of this work, therefore, is to use alcohol with different molecular structures as a surfactant to systematically clarify the mechanism by which the different number and positions of functional groups and different lengths of the main chain and the side chain of surfactant affects solid–liquid interfacial heat transfer, and to determine the specific molecular structure of surfactant that can effectively enhance the solid–liquid interfacial heat transfer.

In the present study, non-equilibrium molecular dynamic (NEMD) simulations were performed on the system where the liquid of linear alkane solvent (tetracosane, $C_{24}H_{50}$) containing alcohol surfactant with different molecular structures was placed between two hydrophilic silica surfaces. Alkanes are widely employed as TIM [16], and silica commonly serves as dielectric layers of microelectronic components [17]. Alcohol can strongly interact with many different substances because they are both hydrophilic and hydrophobic and is frequently used to modify surfaces in many fields including the biological membrane [18] and the manufacturing of electrochemical devices [19]. In order to shed light on the molecular mechanisms of heat conduction at the interface and its dependence on the structural and adsorption dynamics characteristics of surfactant molecules, we chose primary and secondary monohydric alcohols, straight-chain and branched-chain dihydric alcohols with different main chain or the side chain length as polymer surfactants. We characterized the molecular arrangement and structure of different surfactants at the interface region, from which we extracted the specific intermolecular interactions affecting the adsorption amount and contribution to heat transfer. We found a special temperature-sensitive surfactant with a specific molecular structure. Temperature-sensitive surfactants are usually used for phase separation [20,21], while the new one we found can be applied to control the interfacial heat transfer by changing its adsorption amount according to the interfacial temperature.

The paper is organized in three sections. The models and simulation methods are presented in Section 2. The results are split in Section 3.1 for the analysis of adsorption amount and arrangement of surfactant molecules, Section 3.2 for the analysis of thermal boundary resistance, and Section 3.3 for molecular-scale heat transfer analysis. Finally, conclusions are drawn in Section 4.

2. Simulation methods

2.1. Molecular model

In the present study, four types of alcohol, examples in the bottom panel of Fig. 1, were chosen as surfactants: primary alcohol (1-Alco), secondary alcohol (2-Alco), straight-chain dihydric alcohol (S-Diol), and branched-chain butanediol (B-Diol). The surfactant chain length influence on adsorption and heat transfer was investigated by varying the alkyl chain lengths of 1-Alco, 2-Alco, and S-Diol from 4 to 32, and varying the side chain length of B-Diol from 8 to 32, as emphasized by the blue color in the bottom panel of Fig. 1. For convenience, we used the number of carbon atoms in an alkyl chain (#C) to represent the length of the alkyl chain of 1-Alco, 2-Alco, and S-Diol, and that of the side chain of B-Diol. A 1-Alco molecule contains one hydroxyl (—OH) group bonded on the primary carbon atom, and a 2-Alco molecule contains one —OH group bonded on the secondary carbon atom at #C/2, close to the center of the alkyl chain. A S-Diol molecule contains two —OH groups bonded on both ends of the chain. A B-Diol molecule contains two —OH groups bonded on both ends of the main chain, where the side chain branches out at carbon 2. The main chain length is 4 for all B-Diol molecules even though the side change can be longer than the main one.

The NERD force field [22–25] was used as the model for alcohol surfactants and tetracosane solvent. This model is a united-atom model, where hydroxyl H and O atoms of alcohol, and a single alkyl group ($—CH_n$) are modeled as a single interaction site. United-atom models have been reported to perform much better than all-atom models when characterizing the liquid structural properties for n-butanol [26] and 1,4-butanediol [27] and thermal conductivity for alcohol and polymer liquid [28]. Thus, the united-atom force field was considered appropriate for the current purpose to model the adsorption behavior of alcohol surfactant affecting the thermal energy transfer. Since the NERD force field only provides the parameters for linear alcohols [22], linear-alkanes [24,25], and branched-alkanes [23], in order to study the thermal property of alcohol surfactant with different molecular structure and obtain comparable results with linear alcohols, parameters for 2-Alco, S-Diol, and B-Diol were obtained by combining the NERD force field parameters for linear alcohols and branched-alkanes. The specific potential parameters used in the present study are listed in the Supporting Information (Table S1), and the method of combining NERD parameters for 2-Alco, S-Diol, and B-Diol is similar to that used in the TraPPE force filed [29,30]. In addition, we carried out additional calculations for various alcohols at #C = 4, and found that the deviations in liquid density from experimental data for 1-butanol [31], 2-butanol [31], and 1,4-butanediol [32] at 293.15 K were less than 3.9%, and the deviations in thermal conductivity for 1-butanol and 2-butanol at 293.15 K [31], and 1,4-butanediol at 333 K [33] were less than 4%. Although it is difficult to verify all the parameters due to the limited experimental data, we consider that our extension of NERD force field to branched-chain alcohols is reasonably sound to clarify the relationship between molecular heat transfer mechanisms and the molecular structure of surfactant.

Silica with hydrophilic silanol surface modification (Si-OH) was used as a solid surface because alcohol surfactants prefer to form hydrogen bonds with silanols and readily form adsorption layers [34] when compared to silane surface modifications (Si-H), also demonstrated in our previous work [10]. The force field for the silica is an all-atom model developed by Lopes [35] from the CHARMM empirical force field, which has been successfully used to determine the structure and dynamic behavior of hydrated materials [36]. The force field parameters are provided in the Supporting Information (Table S2). The silica-surfactant, silica-solvent, and surfactant-solvent interactions were modeled by Lennard-Jones (LJ) potential, where LJ parameters were obtained by using the Lorentz-Berthelot combing rules, similar to previous studies on silica-alkane interface [37,38].

2.2. Simulation process and analysis procedure

Here we introduce the simulation process in brief since it is essentially the same as in our previous paper, where more detailed description of the simulation procedure is provided [10]. LAMMPS [39] was used for all the MD simulations. Initially, the system was enclosed in a box with dimensions of $59 \times 63.6 \times 600$ Å^3, and the periodic boundary condition was applied in the x and y directions. Two silica walls were placed on the left and right sides of the system in the z direction and solvent molecules were placed randomly between the silica surfaces to construct a liquid film. Afterward, alcohol molecules were placed near the silica surfaces, partly overlapping the constructed solvent film. The following equilibration procedure would fully mix the surfactant and solvent to eliminate the influence of the initial artificial placement of liquid molecules. The overall concentration of surfactant, i.e., the mole fraction of surfactant alcohol, $c_{\text{surf}}^{\text{over}}$, was 5% for all the systems.

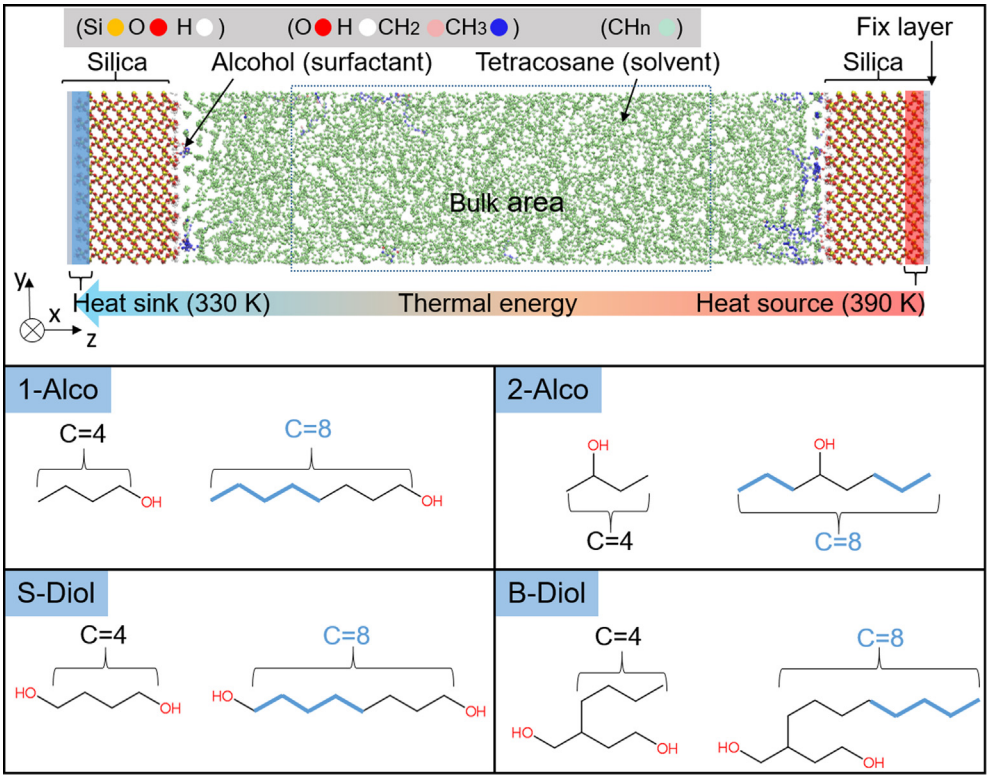

Fig. 1. Side view of the simulation system is shown in the top panel, where a liquid layer consisting of tetracosane (solvent) and alcohol (surfactant) molecules is placed between two hydroxylated silica surfaces. The examples of four types of alcohol when the #C = 4 and 8 are illustrated in the bottom panel. The part of the chain is marked in blue, where chain length is varied as a parameter.

NEMD simulations [40] were performed on the system to investigate heat transfer characteristics. We will refer the silica walls as "left" and "right" in accordance to the Fig. 1 in the z direction. Initially, a temperature annealing process that consists of a volume shrinkage step and a fluctuation step was carried out at least 8 times for a total run of 10 ns to sufficiently disperse surfactant molecules into the solvent. Afterwards, the temperatures of the outmost O layers of silica walls on the left and right sides were set to 330 K as a heat sink and 390 K as a heat source, respectively, by Langevin thermostat with a damping coefficient of 100 fs. The pressure of the system was controlled at 1 atm by fixing the outmost Si layer of the left silica wall and subjecting a constant force to the outmost Si layer of the right silica wall in the z direction for a run of 20 ns. The z dimension of the system was obtained as shown in Tables 1 and 2. Finally, the outmost Si layers of silica walls on the right side were fixed, and the simulation with the same temperature setting was continually carried out for 80 ns. We carried out one long-time simulation for each kind of surfactant to estimate the number density and other properties. Because the surfactant adsorption due to hydrogen bond at the interface is a dynamic process where both the adsorption and desorption occurs, the interfacial density will reach constant value after a long-time simulation when a certain adsorption capacity has been reached. The analysis data was collected from the last 60 ns after the 20 ns equilibration for the system to reach a non-equilibrium steady state under constant heat flux J_{in}. The magnitude of the heat flux induced to the system across a control surface with surface area S_{xy} was obtained as follows [41]:

$$J_{\text{in}} = \frac{E^{\text{source}} - E^{\text{sink}}}{2S_{xy}t} \tag{1}$$

where E^{source}, and E^{sink} are the kinetic energy added in the heat source and subtracted from the heat sink over time t by Langevin thermostat, respectively.

The thermal boundary resistance at the silica-liquid interface, R_{b}, was evaluated by

$$R_{\text{b}} = \frac{\Delta T}{J_{\text{in}}}, \tag{2}$$

where temperature jump $\Delta T$is the difference between the temperature of a silica wall and liquid at the interface, which was obtained by the linear extrapolation method as described in our previous study [10].

Table 1
Simulation conditions for the cases with primary alcohol (1-Alco) and secondary alcohol (2-Alco) as a surfactant at mole fraction of $c_{\text{surf}}^{\text{over}}$ = 5%.

#C (1-Alco)	z-dimension [Å]	c_{surf}^{bulk}	Bulk density of the liquid [g/cm^3]	#C (2-Alco)	z-dimension [Å]	c_{surf}^{bulk}	Bulk density of the liquid [g/cm^3]
4	235.30	1.24%	0.740	4	235.12	0.46%	0.740
8	236.71	1.17%	0.741	8	236.66	1.71%	0.740
16	239.46	1.74%	0.740	16	239.59	1.47%	0.742
24	242.03	1.36%	0.741	24	242.34	3.49%	0.741
32	245.17	1.24%	0.742	32	245.17	2.50%	0.743

Table 2
Simulation conditions for the cases with straight-chain diol (S-Diol) and branched-chain butane diol (B-Diol) as a surfactant at mole fraction of c_{surf}^{over} = 5%.

#C (S-Diol)	z-Dimension [Å]	c_{surf}^{bulk}	Bulk density of the liquid [g/cm^3]	#C (B-Diol)	z-Dimension [Å]	c_{surf}^{bulk}	Bulk density of the liquid [g/cm^3]
4	234.87	0.05%	0.741	4	236.67	2.51%	0.742
8	236.54	0.04%	0.741	8	238.04	3.50%	0.743
16	239.51	0.10%	0.742	16	240.98	0.99%	0.743
24	242.25	0.41%	0.741	24	243.34	3.11%	0.743
32	245.04	0.30%	0.742	32	246.48	3.62%	0.744

The heat flux in the z direction J_z across a control surface with surface area S_{xy} in the z-direction can be expressed for n-body potentials as follows [42]:

$$J_z S_{xy} = \sum_s E_s \frac{v_{z,s}}{|v_{z,s}|} n_s^* + \sum_{\substack{\text{all } n\text{-body} \\ \text{potential}}} \sum_{s_1} \sum_{s_1>s_2} \cdots \sum_{s_n>s_{n-1}} \left[\frac{1}{n} \sum_{\alpha=1}^{n-1} \sum_{\beta=\alpha+1}^{n} (\boldsymbol{F}_{s_\alpha,U} \cdot \boldsymbol{v}_{s_\alpha} - \boldsymbol{F}_{s_\beta,U} \cdot \boldsymbol{v}_{s_\beta}) \{H(z_{s_\alpha} - z_{xy}) - H(z_{s_\beta} - z_{xy})\} \right], \quad (3)$$

where the first term on the right side represents the sum of kinetic and potential energy due to the movement of site s, and the second term represents the heat flux due to inter- and intramolecular (stretching, angle, and torsion) interactions. In this equation, n_s^* is 1 or 0 depending on if site s has crossed S_{xy} during a single time step, $v_{z,s}$ and $\mathbf{v}_s$ is the z component of velocity and velocity vector of site s, respectively, $\mathbf{F}_{s,U}$ and z_s is the force exerted on site s due to n-body potential energy U and z-coordinate of site s, and Heaviside step function $H(x)$ is 0 if x less than 0 or 1 if x larger than 0. The decomposition of heat flux in a control volume can be obtained by integrating Eq. (3) along the direction perpendicular to the control surface [42]. For calculation details refer to our previous study [10].

The detailed conditions for each system are summarized in Tables 1 and 2, where the equilibrium mole fractions of alcohol in the bulk area, c_{surf}^{bulk}, were measured in the area away from a silica further than 50 Å as defined in Fig. 1. The equations of motion were time-integrated by a standard Velocity Verlet algorithm with a time step of 0.5 fs. Coulomb interactions were calculated by the Particle-Particle-Particle-Mesh (PPPM) approach [43] with a relative force accuracy of 10^{-5} and a real space cut-off radius of 12 Å, where the method of applying non-periodic boundary condition in the z direction on the system is provided by Yel et al [44]. The cutoff distance for LJ potential was also set as 12 Å. RATTLE algorithm [45] was used to constrain the O-H bonds of silanols. The USER-INTEL package [46] in LAMMPS was used to deal with long-range Coulomb interaction in order to enhance computational efficiency.

3. Results and discussion

3.1. Adsorption amount and molecular arrangement

The site number density profile of 1,4-butanediol surfactant, tetracosane solvent, and silica wall are shown in Fig. 2 as an example. The positions of "Interlayer 1" and "Interlayer 2" are defined at the coordinates of the closest and second-closest number density minimum of solvent to the silica surface. The first (1st) and second (2nd) adsorption layers are defined as between the silica surface and "Interlayer 1", and between "Interlayer 1" and "Interlayer 2", respectively. We defined the area number densities of adsorbed molecules to qualify the adsorption amount, which was obtained by integrating the number density of corresponding interaction sites in the 1st adsorption layer in the z direction.

The area number density of hydroxyl (—OH) groups and alkyl (—CH_n) groups of different alcohol surfactants in the 1st adsorption layer is plotted against #C on the cold and hot sides as shown in Fig. 3, where the cold and hot sides correspond to the left and right sides in Fig. 2, respectively. The simulation snapshots at the interface for different alcohol cases are shown in Fig. 4. We also calculated the orientation order parameter $P(z)$ to quantify the orientation of alcohol molecules with respect to the z-axis (the normal of the silica surface) as follows [48]:

$$P(z) = \frac{1}{2}\left\langle 3\cos^2\theta_{i-(i+2)}^z - 1 \right\rangle \quad (4)$$

where the angle bracket indicates the ensemble average, and $\cos\theta_{i-(i+2)}^z$ is given by

$$\cos\theta_{i-(i+2)}^z = \frac{\boldsymbol{u}_z \cdot \boldsymbol{u}_{i-(i+2)}}{|\boldsymbol{u}_z||\boldsymbol{u}_{i-(i+2)}|} \quad (5)$$

where $\boldsymbol{u}_z/|\boldsymbol{u}_z|$ is the unit vector in the z direction, $\boldsymbol{u}_{i-(i+2)}/|\boldsymbol{u}_{i-(i+2)}|$ is the unit vector of the connecting line between ith site and $(i+2)$th site whose definition is illustrated in Fig. S1 in the Supporting Information, and the corresponding z-coordinate for $P(z)$ is the midpoint between ith site and $(i+2)$th site in the z-direction. The value of $P(z)$ ranges from − 0.5 to 1, where a positive value corresponds to an orthogonal arrangement of molecules to the z-axis, while a negative value corresponds to a parallel arrangement of molecules to the z-axis, and zero value corresponds to randomly oriented molecules. For the cases with different surfactant alcohols when #C = 16, the orientation order parameter $P(z)$ of alcohol and the number density profiles of the interaction sites of alcohol, solvent, and silica are shown in Fig. 5 as an example, and other cases are shown in Section 2 of the Supporting Information.

For all types of alcohol, the amount of adsorbed —OH groups does not substantially change with increasing chain length as shown in Fig. 3A and B, while the amount of adsorbed —CH_n groups increases as shown in Fig. 3C and D. In other words, for the same type of surfactant, the amount of adsorbed alcohol molecules remains almost constant independently of chain length, which indicates the adsorption is mostly affected by the —OH groups

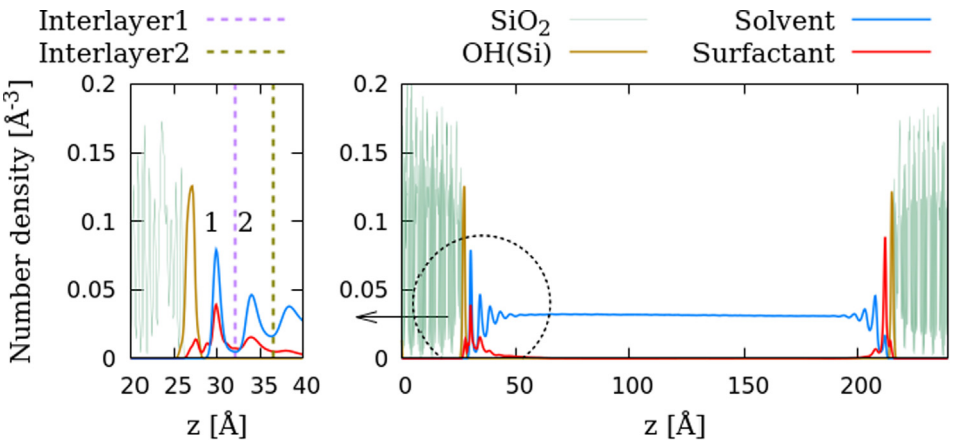

Fig. 2. The site number density profile of 1,4-butanediol (S-Diol) surfactant molecules, tetracosane solvent molecules, and silica walls with silanol surface modification. The left panel shows the locations of the first (1st) and second (2nd) adsorption layers. The positions of "Interlayer 1" and "Interlayer 2" are also shown as dashed vertical lines.

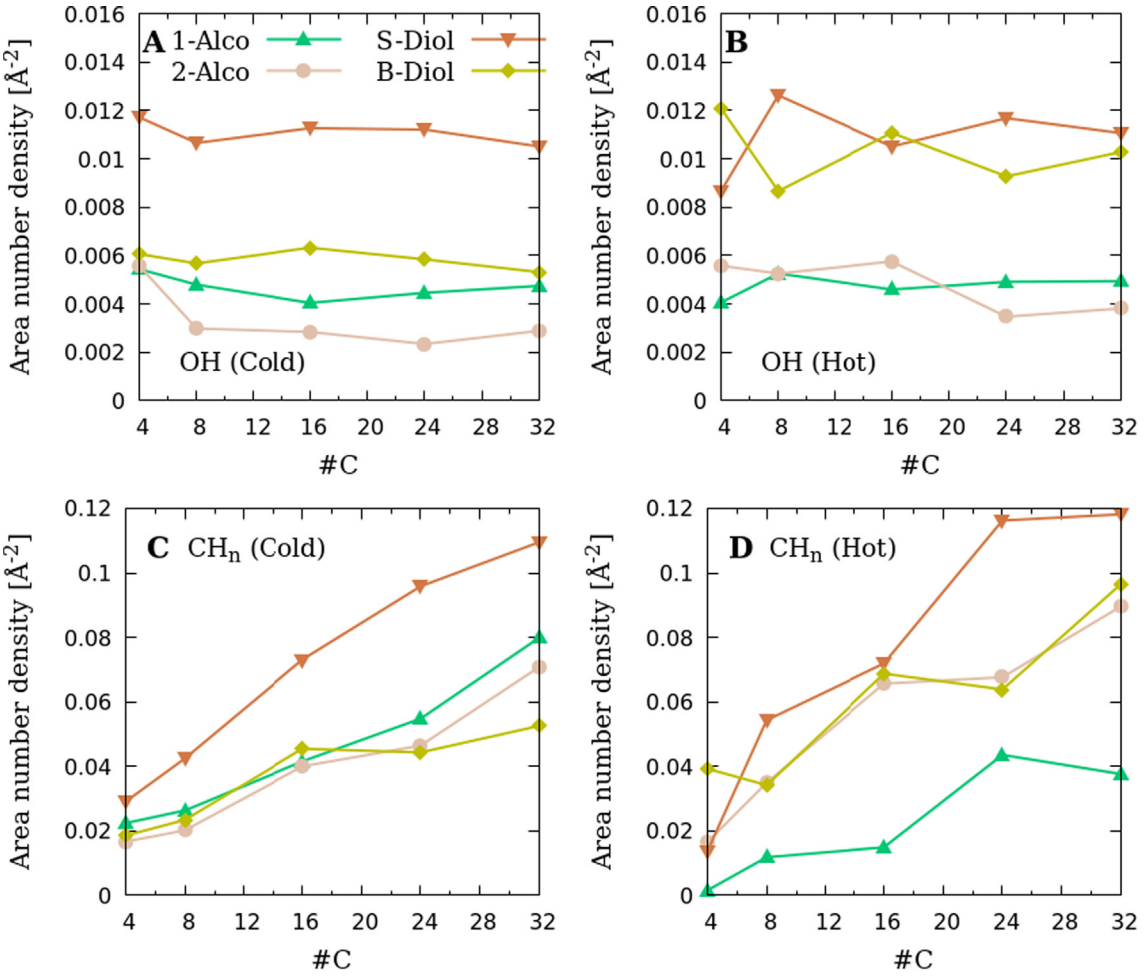

Fig. 3. Area number density of (A, B) hydroxyl (—OH) groups and (C, D) alkyl groups (—CH_n) in 1-Alco, 2-Alco, S-Diol, and B-Diol molecules in the 1st adsorption layer near the Si-OH surfaces on cold and hot sides as a function of #C. The error bars were calculated by the block average method [47] where the last 20 ns of the simulation is evenly divided into 5 blocks. The calculated error bars were too small to be observable.

rather than the alkyl chain. According to the peak positions of density profiles in Fig. 5, for all the surfactant cases, peak positions of density profiles are located in the order of hydroxyl H, O, and —CH_a groups. Therefore, according to our definition of $P(z)$ for each surfactant in the above paragraph and in the Supporting Information (Fig. S1), $P(z)$ near the silica surface is mostly contributed by the tilt of connecting line between hydroxyl H and —CH_a groups, quantifying the orientation of —CH_aOH groups. For 1-Alco, 2-Alco, and S-Diol, the orientation parameter value is close to 1 between the density peaks of hydroxyl H and —CH_a groups, which means that most —CH_aOH groups are orientated vertically. In case of B-Diol, the orientation parameter value is close to 0 between the density peaks of

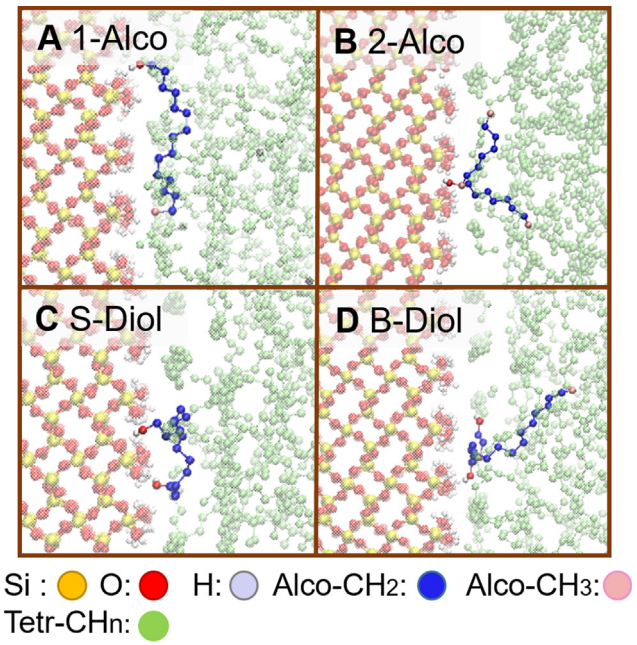

Fig. 4. Snapshots of alcohol surfactant molecules adsorbed at silica-solvent interface on the cold side for the cases of 1-Alco, 2-Alco, B-Diol, and S-Diol with #C = 16.

hydroxyl H and —CH_a groups, which means that most —CH_aOH groups are orientated randomly. The low density distribution at the peak position of $P(z)$ near the silica surface for B-Diol means that only a small amount of —CH_aOH groups that very close to the silica surface shows vertical orientation, while the orientation of CH_aOH groups become more random when slightly far away from silica surface. This adsorption phenomenon can be observed in Fig. 4.

Although in most cases the adsorption amount of —OH groups of 2-Alco is close to that of 1-Alco (Fig. 3A, B), the adsorption structure for 1-Alco and 2-Alco is different as shown in Fig. 4A and B. From the density profile in Fig. 5, compared with 1-Alco, 2-Alco shows a greater distance between Si and —OH groups and a larger overlapping area between alcohol CH_a groups and solvent, which indicates that the adsorbed "—CH_aOH" groups of 2-Alco are further away from the silica surface and closer to the first solvent adsorption layer. The structural analysis also shows that adsorbed 2-Alco tilt farther from silica surface compared with 1-Alco, where an average angle between the z-axis and OH bond θ^z_{H-O} ranges from 62° to 71° for 2-Alco while this angle is almost kept at 55° for 1-Alco.

The number of adsorbed —OH groups in S-Diol is about 2.4 times larger than that of 1-Alco as shown in Fig. 3A and B, which indicates a second —OH group in the alcohol molecule significantly increases the adsorption amount of functional groups. Desbene et al. proposed that the adsorption behavior of nonionic surfactant is determined by a combination of the primary and secondary

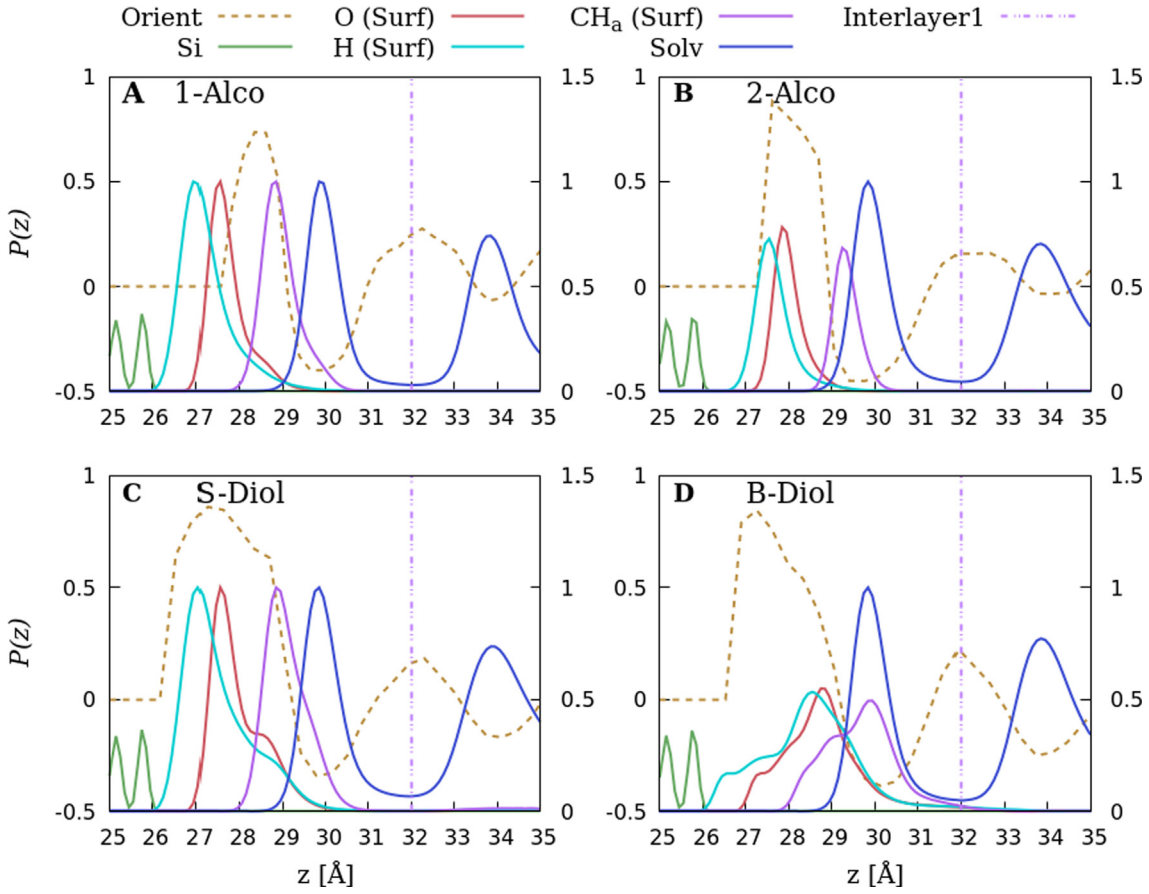

Fig. 5. Orientation distributions (left axis) of alcohol molecules and normalized number density distributions (right axis) of the hydroxyl H and O, and —CH_a groups (—CH_n groups adjacent to hydroxyl O) of alcohol, silica, and solvent for the cases of 1-Alco, 2-Alco, S-Diol, and B-Diol on the cold side when #C = 16. The 1st adsorption layer is defined as between the silica and "Interlayer 1".

adsorption mechanisms, that is, a direct interaction between solid-philic component of the surfactant and the solid surface, and a lateral interaction between the surfactant molecules, respectively [49]. The high adsorption amount of S-Diol is mostly due to the primary adsorption mechanism. Wider adsorption density layers of —OH groups in S-Diol and B-Diol than that in 1-Alco is observed in Fig. 5, which is mostly due to the secondary adsorption, that is in the 1st adsorption layer some neighboring —OH groups in dihydric alcohol molecules cross link with each other instead of directly adsorbing onto silica surface. The short chain S-Diol shows a wider number density of —OH groups than long chain S-Diol as shown in Fig. S3 in the Supporting Information, which indicates that —OH groups of short chain S-Diol cross link easier with neighboring —OH groups of S-Diol in the 1st adsorption layer. An increase in the number of —OH groups in alcohol causing increased adsorption of alcohol molecules on a hydrated surface has also been observed in other works [50].

From the number density profiles on the hot side (Fig. 3B, D), the adsorption amounts of —OH groups for S-Diol and B-Diol are similar, but more —CH_n groups distribute in the 1st adsorption layer for S-Diol than for B-Diol as the chain length increases. This is because in most cases, both —OH groups in one S-Diol molecule are located in the 1st adsorption layer (more than 96% with #C from 4 to 24 and about 71% with #C = 32), thereby alkyl chain between —OH groups of S-Diol is mostly limited in the vicinity of silica surface as shown in Fig. 4C, while the side alkyl chain of B-Diol molecule can easily elongate to the bulk liquid as shown in Fig. 4D.

Different from the hot side, B-Diol on the cold side shows much lower adsorption amount of —OH groups than S-Diol as shown in Fig. 3A. It is considered that the different adsorption amount of surfactant is a result of the balance of the interaction strength between solid-surfactant, surfactant-solvent, and solid-solvent. S. Partyka et al. found the adsorption of nonionic surfactant increases at the water–solid interface with increasing the temperature [51]. They proposed that because the adsorption of water is lower at the higher temperature, water solvent is displaced easily from the solid surface at the higher temperature. In our cases, the adsorption of alkane solvent onto Si-OH surface is also lower when interfacial temperature is higher [37,38]. Making the same assumption for solid-solvent interface, it is reasonable to consider that easier displacement of alkane solvent is responsible for the high adsorption of B-Diol surfactant on the hot side. Regarding the cold side, the adsorption of alkane solvent onto silica surface becomes stronger at the lower interfacial temperature, thereby the adsorption competition between surfactant and solvent might occur. However, only B-Diols show much smaller adsorption on the cold side than on the hot side, while no distinct change is observed for S-Diol on both sides. Previous work indicated that surfactant adsorption is mostly affected by surfactant-solvent interactions when the temperature closes to the lower consolute phase boundary [52]. Since B-Diols have higher solvent affinity than S-Diols due to their adsorption structure as we discussed in the last paragraph and in Section 3 of the Supporting Information, B-Diol is easier to be attracted by the surrounding solvent molecules than S-diols. In addition, the interfacial density of solvent is higher at lower interfacial temperature, which means there are more solvent molecules that can attract the adsorbed surfactant on the cold side. As a result, the adsorption amount of B-Diols decreases obviously and becomes much less than S-Diols on the cold side.

3.2. Thermal boundary resistance

Thermal boundary resistance R_b for different alcohol surfactants is plotted against #C in Fig. 6. As chain length increases, R_b distinctly decreases for 1-Alco, S-Diol, and B-Diol molecules, while no obvious decrease in R_b is observed for 2-Alco. From the structure analysis in Section 3.1, we found adsorbed "—CH_aOH" groups in 2-Alco are farther away from the silica surface than that in 1-Alco and dihydric alcohols. A previous study [53] indicated that the hydrogen bond mostly contributed to interfacial heat transfer indirectly, by decreasing intermolecular distance and thereby increasing repulsive vdW interaction. Therefore, compared with 1-Alco, the higher R_b for 2-Alco can be attributed to the larger distance between silica and adsorbed "—CH_aOH" groups of 2-Alco, which will be discussed later.

Different from our expectation, although S-Diol shows much higher adsorption amount of —OH groups than that of 1-Alco (Fig. 3), the performance of S-Diol surfactant on reducing R_b is not much better than that of 1-Alco as shown in Fig. 6, especially for the short-chain surfactant. This indicates that not only the number of functional groups in surfactant molecule is important for interfacial heat transfer, but also adsorption structure should be considered which will be discussed in Section 3.3.

Although most of liquids show higher interfacial density on the cold side than on the hot side near the solid surface [54], B-Diol show higher adsorption amount on the hot side than on the cold side as we discussed in Section 3.1. Due to this, the cases of B-Diol show much lower R_b on the hot side. Such reverse temperature-sensitive property allows B-Diol surfactant to significantly enhance interfacial heat transfer with increasing the interfacial temperature. B-Diol is also the best surfactant on reducing R_b compared with other surfactants on the hot side, which relates to the surfactant-solvent heat transfer and will be discussed in the next section.

3.3. Molecular-scale heat transfer analysis

In order to clarify the heat transfer from silica surface to alcohol and how the thermal energy finally diffuses into solvent, heat flux across the silica-liquid interface is decomposed into silica-surfactant and silica-solvent intermolecular contributions based on Eq. (3) as shown in Fig. 7A. The breakdown of heat flux across liquid–liquid interlayer ("Interlayer1" in Fig. 2) is shown in Fig. 7B, where the intermolecular contributions between surfactant in the 1st adsorption layer (1) and surfactant in the bulk area (bulk), between surfactant (1) and solvent (bulk), between solvent (1) and solvent (bulk), and between solvent (1) and surfactant (bulk) are separately shown. The calculation details are provided in our previous study [10].

Fig. 7 takes the cases of S-Diol as an example because the dependence of decomposition of heat flux on surfactant chain length is similar for all surfactants. As the surfactant chain length increases, the vdW and Coulomb intermolecular heat transfer between silica and surfactant ("Si-Surf (vdW)" and ("Si-Surf (Coul)" in Fig. 7A) across the silica-liquid interface increase, and gradually exceed the heat transfer amount between silica and solvent ("Si-Solv (vdW)" in Fig. 7A). Additionally, trends of increasing vdW intermolecular heat transfer between surfactant and solvent ("Surf (1)-Solv (bulk)" in Fig. 7B) across interlayer for surfactant chain longer than 8 have not been particularly clear for S-Diol, unlike our previous study [10] where the trends were clearly observed for 1-Alco across all chain lengths. This is because compared with 1-Alcos, the alkyl chains of S-Diols distribute more in the first adsorption layer as shown in Fig. 3C, in other words, the alkyl chains of S-Diols prefer to spread onto the surface rather than elongate to the bulk liquid, which results in less contact area with solvent, and Surf (1)-Solv (bulk) does not increase apparently with #C past 8. Moreover, "other" term in Fig. 7B consists of the contribution from intramolecular interaction (bond stretching, angle bending, and torsion interaction in surfactant and solvent molecules), that from silica-liquid intermolecular interaction, and energy

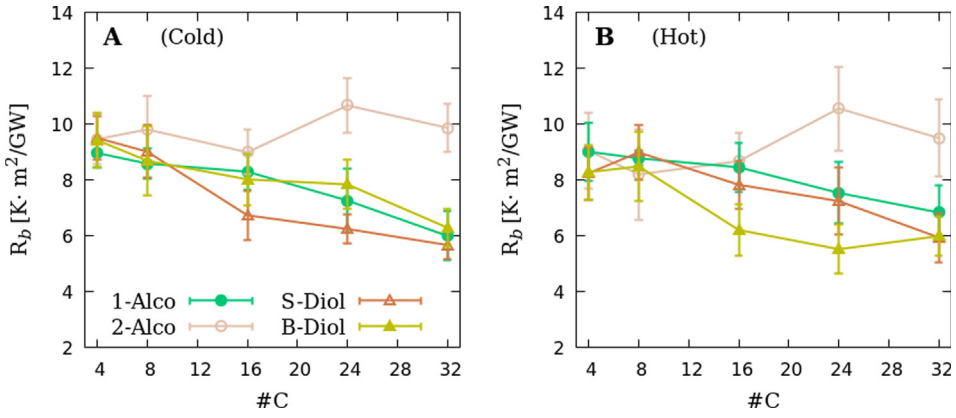

Fig. 6. Thermal boundary resistance R_b for the cases with different alcohol surfactant on the (A) cold and (B) hot sides as a function of #C. Error bars display the standard error of the mean estimated by the block average method [47] where the data is evenly divided into 6 blocks.

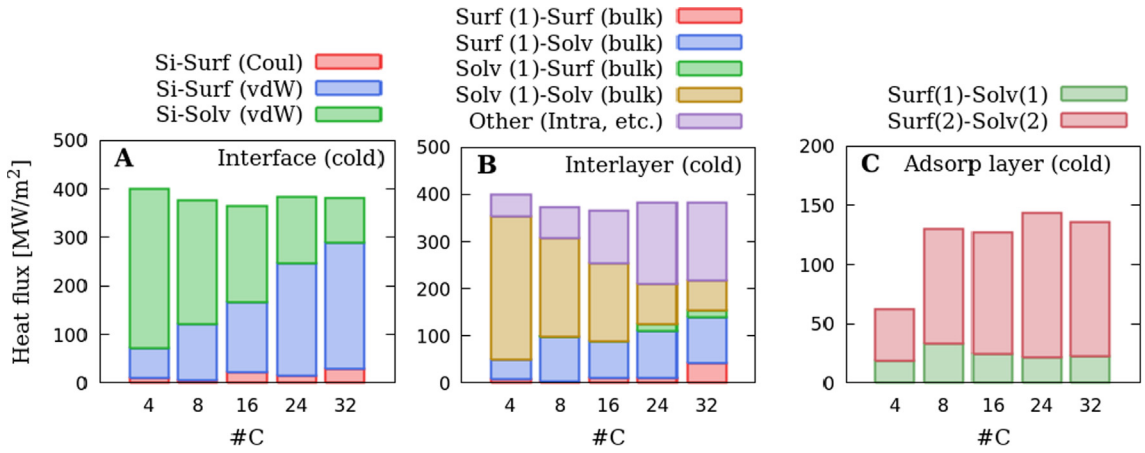

Fig. 7. The interaction contribution to heat flux (A) across the solid–liquid interface, (B) across the liquid–liquid interlayer (Interlayer 1), and (C) between alcohol surfactant and tetracosane solvent in the 1st and 2nd adsorption layers on the cold side for the cases of S-Diol with #C from 4 to 32.

transfer via molecular migration at the interlayer, where the first term is dominant, and the last two terms are negligibly small. Similar to our previous study for 1-Alco [10], with increasing the S-Diols surfactant chain length, more alkane solvent near the solid surface is replaced by alkyl chain of surfactant. This replacement explains why the "other" term, which is mostly contributed by intramolecular interaction, increases with the surfactant chain length as shown Fig. 7B. Thus, the increasing trend of this term indicates that the intramolecular heat transfer along the surfactant chain increases as surfactant chain becomes longer.

The components of heat flux due to the intermolecular interaction between surfactant and solvent molecules in the 1st or 2nd adsorption layers were calculated as shown in Fig. 7C. The 1st and 2nd adsorption layers are defined in Section 3.1 as shown in Fig. 2. For all types of alcohol surfactants, the heat transfer from surfactant to solvent in the 2nd adsorption layer ("Surf(2)-Solv (2)" in Fig. 7C) is larger than that that in the 1st adsorption layer ("Surf(1)-Solv(1)" in Fig. 7C), which indicates that the exchange of thermal energy between surfactant and solvent is more efficient in the 2nd adsorption layer than in the 1st adsorption layer. It also can be observed from the larger temperature difference between surfactant and solvent in the 2nd adsorption layer than that in the 1st adsorption layer as shown in Fig. S6 in the Supporting Information. This is because that the heat is mostly transferred from silica surface to —OH groups of surfactants due to hydrogen bond and then along the alcohol molecular chains to the —CH_n groups of surfactant in the 2nd adsorption layer due to intramolecular heat transfer. The excellent heat conduction along the alcohol molecular chains [55] result in the temperature of surfactant in the 2nd adsorption layer is close to that in the 1st adsorption layer. Nevertheless, the heat transfer between flat arranged solvent adsorption layers is mostly contributed by their intermolecular interaction, which is not as efficient as the heat transfer in surfactant. As we discussed in Section 3.1, compared with S-Diol, adsorbed B-Diol molecules prefer to elongate to the bulk liquid instead of distributing in the 1st adsorption layer, which results in more efficient surfactant-solvent intermolecular heat transfer. As a result, B-Diol shows lower R_b than S-Diol at the similar adsorption amount on the hot side as shown in Fig. 6B.

The interfacial thermal conductance (ITC) is the inverse of R_b defined by Eq. (2). The silica-surfactant partial ITC can be obtained by dividing the silica-surfactant interaction contribution to heat flux by the temperature jump as $(J_{vdW}^{si\text{-}surf} + J_{Coul}^{si\text{-}surf})/|\Delta T|$. Then we further divided silica-surfactant partial ITC by the area number density of interaction site of surfactant (H, O, CH_n) in the 1st adsorption layer, so that per-site surfactant contribution to partial ITC is obtained and plotted in Fig. 8 for 1-Alco and S-diol. Compared with 1-Alco, S-diol shows lower site contributions to ITC, which indicates that the average thermal enhancement per S-diol molecule is not as large as that of each 1-Alco molecule. This is mostly because that although S-Diol shows much higher adsorption amount of —OH groups than 1-Alco (Fig. 3), not all of those

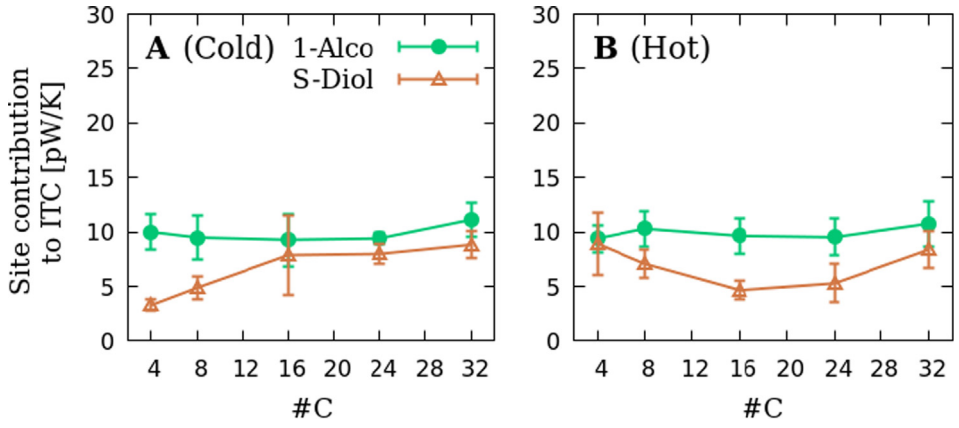

Fig. 8. Average site contributions of alcohol to ITC as a function of #C (A) on the cold side and (B) on the hot side for the cases of 1-Alco and S-diol. The standard error of mean estimated by the block average method [47] where the data is evenly divided into 6 blocks.

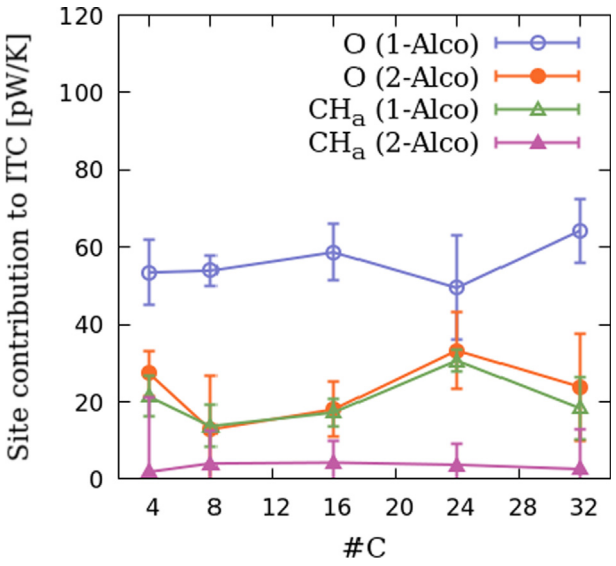

Fig. 9. ITC due to each hydroxyl O or —CH_a group (—CH_n groups adjacent to hydroxyl O) contributions of 1-Alco and 2-Alco on the hot side with #C from 4 to 32. The standard error of mean estimated by the block average method [47] where the data is evenly divided into 6 blocks.

—OH groups form direct hydrogen bonds with silica surface, especially for short chain S-Diol as we discussed in Section 3.1. Therefore, —OH groups of S-Diol that cross link with other S-Diol —OH groups in the 1st adsorption layer cannot effectively contribute to interfacial heat transfer.

In addition, the intramolecular interaction contribution to heat transfer at the interlayer for the case of S-Diol becomes higher than that of 1-Alco when the surfactant chain length increases as shown in Fig. S5 of the Supporting Information. In other words, the second adsorbed —OH groups of surfactant molecules effectively improve the intramolecular heat transfer only when the surfactant chain is longer than 8. It is expected that S-Diol would reduce R_b more effectively than 1-Alco when its chain length becomes much longer.

In order to investigate the difference in heat transfer between the cases of 1-Alco and 2-Alco, each contribution of hydroxyl O and the —CH_a group of 1-Alco and 2-Alco to partial ITC are obtained and plotted in Fig. 9 on the hot side. The data on the cold side is not shown here due to their similarity to the hot side. In addition, the heat transfer from silica to the hydroxyl H of alcohol is negligibly small due to the weak interaction strength and mismatch of frequency vibration between H atoms and silica surface [56,57] and thereby not calculated in the present study. The contributions to ITC from each hydroxyl O and —CH_a group of 2-Alco are clearly lower than those of 1-Alco, which indicates that the energy transfer from silica surface to adsorbed "—CH_aOH" groups of 2-Alco is not as efficient as that of 1-Alco. This phenomenon results from the difference in the adsorption arrangement of the surfactant molecule as we discussed in Section 3.1, where the long distance between silica surface and adsorbed "—CH_aOH" groups of 2-Alco prevents the efficient heat transfer from silica to surfactant. As a result, for the cases of 2-Alco, although the heat path from silica via surfactant to solvent becomes dominant as the surfactant chain length increases (Fig. 7), R_b is not reduced (Fig. 6).

4. Conclusions

This paper focused on the investigation of the effect of the number and the position of hydroxyl groups and the length of the main chain and side chain in the organic surfactant molecules on the silica-alkane interfacial heat transfer by MD simulation. Linear primary alcohol, secondary alcohol, straight-chain diol, and branched-chain diol with different chain lengths as organic surfactants were compared.

Overall, thermal boundary resistance R_b was mostly determined by the adsorption amount and the molecular arrangement of surfactant at interface region, which was a result of the competition between the silica-surfactant, silica-solvent, and solvent-surfactant interactions. The increase in the adsorption amount or the number of functional groups of surfactant does not necessarily increase the interfacial heat transfer. Primary hydroxyl groups of alcohol showed the perpendicular binding mode onto silica surface, which produced an efficient microscopic heat path from silica to surfactant. However, secondary hydroxyl groups of alcohol resulted in a larger distance from silica surface, which prevented efficient interfacial heat transfer. Due to this, secondary alcohol surfactants hardly reduce R_b. Compared with linear monohydric alcohols, linear dihydric alcohols showed higher adsorption amount because multiple hydroxyl groups have a stronger aggregation effect on alcohol molecules in the adsorption layer due to Coulomb interaction. However, the performance of linear dihydric alcohols on the reduction of R_b was on par with linear monohydric alcohols. This is because not all —OH groups of linear dihydric alcohol can form direct hydrogen bonds with silica surface due to other —OH groups in dihydric alcohol, and the second —OH group increases alcohol intramolecular heat transfer only when alcohol

chain become very long. Compared with linear dihydric alcohol, the branched dihydric alcohol showed higher R_b on the cold side and lower R_b on the hot side. This is because branched dihydric alcohol has a larger preference to bulk liquid, which improves the surfactant-solvent intermolecular heat transfer but leads to the desorption of surfactant at the low interfacial temperature. The branched dihydric alcohol performed better on reducing R_b than other alcohol when the interfacial temperature was high enough to maintain the adsorption amount of surfactant at sufficiently high level. From the application point of TIM, the operating temperature of the power module becomes increasingly high due to continual device miniaturization, for example, some SiC-based electronic devices operate at temperatures as high as 450 °C [58]. Thus we consider the molecule containing two solid-philic terminal functional groups and a solvent-philic long side chain, such as branched dihydric alcohol surfactant, has a great potential application to enhance the substrate-TIM interfacial heat transfer on the high operating temperature environment. Furthermore, the ability to spontaneously enhance heat dissipation rate with increasing interfacial temperature makes such temperature-sensitive surfactant ideal for a number of applications, including some precise electronic devices that lay on the requirement within a limited temperature range. Given the high-efficiency surfactants discovered in the present study and their temperature dependence, we propose that future work is to further improve the molecular structure of such surfactant and to determine its effect on interfacial thermal conductance at various temperature conditions.

Declaration of Competing Interest

The authors declare that they have no known competing financial interests or personal relationships that could have appeared to influence the work reported in this paper.

Acknowledgements

This work was supported by JST CREST Grant Number JPMJCR17I2, Japan. Numerical simulations were performed on the Supercomputer system "AFI-NITY" at the Advanced Fluid Information Research Center, Institute of Fluid Science, Tohoku University.

Appendix A. Supplementary material

Supplementary data to this article can be found online at https://doi.org/10.1016/j.molliq.2021.116243.

References

[1] N. Goel, A. Bhattacharya, J.A. Cervantes, R.K. Mongia, S.V. Machiroutu, Hau-Lan Lin, Ya-Chi Huang, Kuang-Cheng Fan, Bar-Long Denq, Chen-Hua Liu, Chun-Hung Lin, Chi-Wei Tien, Jenq-Haur Pan, Technical review of characterization methods for thermal interface materials (TIM), in: 2008 10th Electronics Packaging Technology Conference, 2008, pp. 1461–1471, https://doi.org/10.1109/EPTC.2008.4763637.

[2] J. Due, A.J. Robinson, Reliability of Thermal Interface Materials: A Review, Appl. Therm. Eng. 50 (1) (2013) 455–463, https://doi.org/10.1016/j.applthermaleng.2012.06.013.

[3] S. Harrell, T. Seidel, B. Fay, The National Technology Roadmap for Semiconductors and SEMATECH Future Directions, Microelectron. Eng. 30 (1) (1996) 11–15, https://doi.org/10.1016/0167-9317(95)00185-9.

[4] I. Firkowska, A. Boden, A.-M. Vogt, S. Reich, Effect of Carbon Nanotube Surface Modification on Thermal Properties of Copper–CNT Composites, J. Mater. Chem. 21 (43) (2011) 17541–17546, https://doi.org/10.1039/C1JM12671G.

[5] I. Jang, K.-H. Shin, I. Yang, H. Kim, J. Kim, W.-H. Kim, S.-W. Jeon, J.-P. Kim, Enhancement of Thermal Conductivity of BN/Epoxy Composite through Surface Modification with Silane Coupling Agents, Colloids Surf., A 518 (2017) 64–72, https://doi.org/10.1016/j.colsurfa.2017.01.011.

[6] S. Ryu, T. Oh, J. Kim, Surface Modification of a BN/ETDS Composite with Aniline Trimer for High Thermal Conductivity and Excellent Mechanical Properties, RSC Adv. 8 (40) (2018) 22846–22852, https://doi.org/10.1039/C8RA03875A.

[7] Z. Ge, D.G. Cahill, P.V. Braun, Thermal Conductance of Hydrophilic and Hydrophobic Interfaces, Phys. Rev. Lett. 96 (18) (2006) 186101, https://doi.org/10.1103/PhysRevLett.96.186101.

[8] Y. Guo, D. Surblys, Y. Kawagoe, H. Matsubara, X. Liu, T. Ohara, A Molecular Dynamics Study on the Effect of Surfactant Adsorption on Heat Transfer at a Solid-Liquid Interface, Int. J. Heat Mass Transf. 135 (2019) 115–123, https://doi.org/10.1016/j.ijheatmasstransfer.2019.01.131.

[9] Y. Guo, D. Surblys, Y. Kawagoe, H. Matsubara, T. Ohara, A Molecular Dynamics Study of Heat Transfer over an Ultra-Thin Liquid Film with Surfactant between Solid Surfaces, J. Appl. Phys. 126 (18) (2019) 185302, https://doi.org/10.1063/1.5123583.

[10] Y. Guo, D. Surblys, H. Matsubara, Y. Kawagoe, T. Ohara, Molecular Dynamics Study on the Effect of Long-Chain Surfactant Adsorption on Interfacial Heat Transfer between a Polymer Liquid and Silica Surface, J. Phys. Chem. C 124 (50) (2020) 27558–27570, https://doi.org/10.1021/acs.jpcc.0c0894010.1021/acs.jpcc.0c08940.s001.

[11] T. Ohtake, N. Mino, K. Ogawa, Effect of Hydrocarbon Chain Length on Arrangement of Chemically Adsorbed Monolayers, Langmuir 8 (9) (1992) 2081–2083, https://doi.org/10.1021/la00045a001.

[12] M. Suttipong, N.R. Tummala, B. Kitiyanan, A. Striolo, Role of Surfactant Molecular Structure on Self-Assembly: Aqueous SDBS on Carbon Nanotubes, J. Phys. Chem. C 115 (35) (2011) 17286–17296, https://doi.org/10.1021/jp203247r.

[13] A. Fabozzi, I. Russo Krauss, R. Vitiello, M. Fornasier, L. Sicignano, S. King, S. Guido, C. Jones, L. Paduano, S. Murgia, G. D'Errico, Branched Alkyldimethylamine Oxide Surfactants: An Effective Strategy for the Design of High Concentration/Low Viscosity Surfactant Formulations, J. Colloid Interface Sci. 552 (2019) 448–463, https://doi.org/10.1016/j.jcis.2019.05.052.

[14] P. Liu, H. Yu, L. Niu, D. Ni, Q. Zhao, X. Li, Z. Zhang, Utilization of Janus-Silica/Surfactant Nanofluid without Ultra-Low Interfacial Tension for Improving Oil Recovery, Chem. Eng. Sci. 228 (2020) 115964, https://doi.org/10.1016/j.ces.2020.115964.

[15] R. Sharma, Small-molecule surfactant adsorption, polymer surfactant adsorption, and surface solubilization: an overview, in: R. Sharma (Ed.), American Chemical Society: Washington, DC, vol. 615, 1996, pp 1–20. doi:10.1021/bk-1995-0615.ch001.

[16] R. Prasher, Thermal Interface Materials: Historical Perspective, Status, and Future Directions, Proc. IEEE 94 (8) (2006) 1571–1586, https://doi.org/10.1109/JPROC.2006.879796.

[17] D.A. Muller, T. Sorsch, S. Moccio, F.H. Baumann, K. Evans-Lutterodt, G. Timp, The Electronic Structure at the Atomic Scale of Ultrathin Gate Oxides, Nature 399 (6738) (1999) 758–761, https://doi.org/10.1038/21602.

[18] A.A. Gurtovenko, J. Anwar, Interaction of Ethanol with Biological Membranes: The Formation of Non-Bilayer Structures within the Membrane Interior and Their Significance, J. Phys. Chem. B 113 (7) (2009) 1983–1992, https://doi.org/10.1021/jp808041z.

[19] K.Y. Suh, A. Khademhosseini, G. Eng, R. Langer, Single Nanocrystal Arrays on Patterned Poly(Ethylene Glycol) Copolymer Microstructures Using Selective Wetting and Drying, Langmuir 20 (15) (2004) 6080–6084, https://doi.org/10.1021/la049217n.

[20] H. Feng, N.A.L. Verstappen, A.J.C. Kuehne, J. Sprakel, Well-Defined Temperature-Sensitive Surfactants for Controlled Emulsion Coalescence, Polym. Chem. 4 (6) (2013) 1842–1847, https://doi.org/10.1039/C2PY21007J.

[21] K.e. Wang, H. Yin, W. Sha, J. Huang, H. Fu, Temperature-Sensitive Aqueous Surfactant Two-Phase System Formation in Cationic−Anionic Surfactant Systems, J. Phys. Chem. B 111 (45) (2007) 12997–13005, https://doi.org/10.1021/jp073903o10.1021/jp073903o.s00110.1021/jp073903o.s002.

[22] R. Khare, A.K. Sum, S.K. Nath, J.J. de Pablo, Simulation of Vapor−Liquid Phase Equilibria of Primary Alcohols and Alcohol−Alkane Mixtures, J. Phys. Chem. B 108 (28) (2004) 10071–10076, https://doi.org/10.1021/jp048144d.

[23] S.K. Nath, R. Khare, New Forcefield Parameters for Branched Hydrocarbons, J. Chem. Phys. 115 (23) (2001) 10837–10844, https://doi.org/10.1063/1.1418731.

[24] S.K. Nath, B.J. Banaszak, J.J. de Pablo, A New United Atom Force Field for α-Olefins, J. Chem. Phys. 114 (8) (2001) 3612–3616, https://doi.org/10.1063/1.1343487.

[25] S.K. Nath, F.A. Escobedo, J.J. de Pablo, On the Simulation of Vapor-Liquid Equilibria for Alkanes, J. Chem. Phys. 108 (23) (1998) 9905–9911, https://doi.org/10.1063/1.476429.

[26] J. Cerar, A. Lajovic, A. Jamnik, M. Tomšič, Performance of Various Models in Structural Characterization of N-Butanol: Molecular Dynamics and X-Ray Scattering Studies, J. Mol. Liq. 229 (2017) 346–357, https://doi.org/10.1016/j.molliq.2016.12.057.

[27] M. Tomšič, J. Cerar, A. Jamnik, Characterization of the Supramolecular Assembly in 1,4-Butanediol, J. Mol. Liq. 259 (2018) 291–303, https://doi.org/10.1016/j.molliq.2018.03.015.

[28] E.A. Algaer, F. Müller-Plathe, Molecular Dynamics Calculations of the Thermal Conductivity of Molecular Liquids, Polymers, and Carbon Nanotubes, Soft Mater. 10 (1–3) (2012) 42–80, https://doi.org/10.1080/1539445X.2011.599699.

[29] B. Chen, J.J. Potoff, J.I. Siepmann, Monte Carlo Calculations for Alcohols and Their Mixtures with Alkanes. Transferable Potentials for Phase Equilibria. 5. United-Atom Description of Primary, Secondary, and Tertiary Alcohols, J. Phys. Chem. B 105 (15) (2001) 3093–3104, https://doi.org/10.1021/jp003882x.

[30] J.M. Stubbs, J.J. Potoff, J.I. Siepmann, Transferable Potentials for Phase Equilibria. 6. United-Atom Description for Ethers, Glycols, Ketones, and

Aldehydes, J. Phys. Chem. B 108 (45) (2004) 17596–17605, https://doi.org/10.1021/jp049459w10.1021/jp049459w.s001.
[31] K. Ogiwara, Y. Arai, S. Saito, Thermal Conductivities of Liquid Alcohols and Their Binary Mixtures, J. Chem. Eng. Japan / JCEJ 15 (5) (1982) 335–342, https://doi.org/10.1252/jcej.15.335.
[32] Q.-S. Li, Y.-M. Tian, S. Wang, Densities and Excess Molar Volumes for Binary Mixtures of 1,4-Butanediol + 1,2-Propanediol, + 1,3-Propanediol, and + Ethane-1,2-Diol from (293.15 to 328.15) K, J. Chem. Eng. Data 53 (1) (2008) 271–274, https://doi.org/10.1021/je700499d.
[33] J.G. Bleazard, T.F. Sun, R.D. Johnson, R.M. DiGuillio, A.S. Teja, The Transport Properties of Seven Alkanediols, Fluid Phase Equilib. 117 (1–2) (1996) 386–393, https://doi.org/10.1016/0378-3812(95)02976-1.
[34] M. Mizukami, M. Moteki, K. Kurihara, Hydrogen-Bonded Macrocluster Formation of Ethanol on Silica Surfaces in Cyclohexane1, J. Am. Chem. Soc. 124 (43) (2002) 12889–12897, https://doi.org/10.1021/ja027141g.
[35] P.E.M. Lopes, V. Murashov, M. Tazi, E. Demchuk, A.D. MacKerell, Development of an Empirical Force Field for Silica. Application to the Quartz−Water Interface, J. Phys. Chem. B 110 (6) (2006) 2782–2792, https://doi.org/10.1021/jp055341j10.1021/jp055341j.s001.
[36] R.T. Cygan, J.-J. Liang, A.G. Kalinichev, Molecular Models of Hydroxide, Oxyhydroxide, and Clay Phases and the Development of a General Force Field, J. Phys. Chem. B 108 (4) (2004) 1255–1266, https://doi.org/10.1021/jp0363287.
[37] H.K. Chilukoti, G. Kikugawa, T. Ohara, Structure and Transport Properties of Liquid Alkanes in the Vicinity of α-Quartz Surfaces, Int. J. Heat Mass Transf. 79 (2014) 846–857, https://doi.org/10.1016/j.ijheatmasstransfer.2014.08.089.
[38] H.K. Chilukoti, G. Kikugawa, M. Shibahara, T. Ohara, Local Thermal Transport of Liquid Alkanes in the Vicinity of α-Quartz Solid Surfaces and Thermal Resistance over the Interfaces: A Molecular Dynamics Study, Phys. Rev. E 91 (5) (2015), https://doi.org/10.1103/PhysRevE.91.052404.
[39] S. Plimpton, Fast Parallel Algorithms for Short-Range Molecular Dynamics, J. Comput. Phys. 117 (1) (1995) 1–19, https://doi.org/10.1006/jcph.1995.1039.
[40] P. Jund, R. Jullien, Molecular-Dynamics Calculation of the Thermal Conductivity of Vitreous Silica, Physical Review B 59 (21) (1999) 13707–13711, https://doi.org/10.1103/PhysRevB.59.13707.
[41] D. Surblys, Y. Kawagoe, M. Shibahara, T. Ohara, Molecular Dynamics Investigation of Surface Roughness Scale Effect on Interfacial Thermal Conductance at Solid-Liquid Interfaces, J. Chem. Phys. 150 (11) (2019) 114705, https://doi.org/10.1063/1.5081103.
[42] D. Torii, T. Nakano, T. Ohara, Contribution of Inter- and Intramolecular Energy Transfers to Heat Conduction in Liquids, J. Chem. Phys. 128 (4) (2008) 044504, https://doi.org/10.1063/1.2821963.
[43] R.W. Hockney, J.W. Eastwood, Computer Simulation Using Particles, Hilger, Bristol, 1988.
[44] I.-C. Yeh, M.L. Berkowitz, Ewald Summation for Systems with Slab Geometry, J. Chem. Phys. 111 (7) (1999) 3155–3162, https://doi.org/10.1063/1.479595.
[45] H.C. Andersen, Rattle: A "Velocity" Version of the Shake Algorithm for Molecular Dynamics Calculations, J. Comput. Phys. 52 (1) (1983) 24–34, https://doi.org/10.1016/0021-9991(83)90014-1.
[46] J. Jeffers, J. Reinders, A. Sodani, Chapter 20 - Optimizing Classical Molecular Dynamics in LAMMPS, in: J. Jeffers, J. Reinders, A. Sodani (Eds.), Intel Xeon Phi Processor High Performance Programming, second ed., Morgan Kaufmann, Boston, 2016, pp. 443–470, https://doi.org/10.1016/B978-0-12-809194-4.00020-X.
[47] M.P. Allen, D.J. Tildesley, Computer Simulation of Liquids, Oxford University Press, 2009.
[48] J.G. Harris, Liquid-Vapor Interfaces of Alkane Oligomers: Structure and Thermodynamics from Molecular Dynamics Simulations of Chemically Realistic Models, J. Phys. Chem. 96 (12) (1992) 5077–5086, https://doi.org/10.1021/j100191a062.
[49] P.L. Desbene, F. Portet, C. Treiner, Adsorption of Pure Nonionic Alkylethoxylated Surfactants down to Low Concentrations at a Silica/Water Interface as Determined Using a HPLC Technique, J. Colloid Interface Sci. 190 (2) (1997) 350–356, https://doi.org/10.1006/jcis.1997.4884.
[50] W. van Bronswijk, H.R. Watling, Z. Yu, A Study of the Adsorption of Acyclic Polyols on Hydrated Alumina, Colloids Surf., A 157 (1) (1999) 85–94, https://doi.org/10.1016/S0927-7757(99)00055-2.
[51] S. Partyka, S. Zaini, M. Lindheimer, B. Brun, The Adsorption of Non-Ionic Surfactants on a Silica Gel, Colloids Surf. 12 (1984) 255–270, https://doi.org/10.1016/0166-6622(84)80104-3.
[52] J.M. Corkill, J.F. Goodman, J.R. Tate, Adsorption of Non-Ionic Surface-Active Agents at the Graphon/Solution Interface, Trans. Faraday Soc. 62 (1966) 979–986, https://doi.org/10.1039/TF9666200979.
[53] T. Zhang, A.R. Gans-Forrest, E. Lee, X. Zhang, C. Qu, Y. Pang, F. Sun, T. Luo, Role of Hydrogen Bonds in Thermal Transport across Hard/Soft Material Interfaces, ACS Appl. Mater. Interfaces 8 (48) (2016) 33326–33334, https://doi.org/10.1021/acsami.6b12073.
[54] A.R.B. Saleman, H.K. Chilukoti, G. Kikugawa, M. Shibahara, T. Ohara, A Molecular Dynamics Study on the Thermal Transport Properties and the Structure of the Solid-Liquid Interfaces between Face Centered Cubic (FCC) Crystal Planes of Gold in Contact with Linear Alkane Liquids, Int. J. Heat Mass Transf. 105 (2017) 168–179, https://doi.org/10.1016/j.ijheatmasstransfer.2016.09.069.
[55] B. Feng, L.-W. Fan, Y. Zeng, Contribution of the Hydroxyl Group on Interfacial Heat Conduction of Monohydric Alcohols: A Molecular Dynamics Study, J. Heat Transfer 142 (3) (2020), https://doi.org/10.1115/1.4045667.
[56] B.-Y. Cao, J.-H. Zou, G.-J. Hu, G.-X. Cao, Enhanced Thermal Transport across Multilayer Graphene and Water by Interlayer Functionalization, Appl. Phys. Lett. 112 (4) (2018) 041603, https://doi.org/10.1063/1.5018749.
[57] H. Sun, Z. Liu, G. Xin, Q. Xin, J. Zhang, B.-Y. Cao, X. Wang, Thermal and Flow Characterization in Nanochannels with Tunable Surface Wettability: A Comprehensive Molecular Dynamics Study, Numer. Heat Transfer, Part A: Appl. 78 (6) (2020) 231–251, https://doi.org/10.1080/10407782.2020.1788849.
[58] T. Funaki, J. Balda, J. Junghans, A. Kashyap, F. Barlow, A. Mantooth, T. Kimoto, T. Hikihara, Power Conversion with SiC Devices at Extremely High Ambient Temperatures, in: 2005 IEEE 36th Power Electronics Specialists Conference, 2005, pp. 2030–2035, https://doi.org/10.1109/PESC.2005.1581911.